A Metastable CaSH₃ Phase Composed of HS Honeycomb Sheets that is Superconducting Under Pressure

Yan Yan, †,‡ Tiange Bi,† Nisha Geng,† Xiaoyu Wang,† and Eva Zurek*,†

Department of Chemistry, State University of New York at Buffalo, Buffalo, NY 14260-3000, USA

E-mail: ezurek@buffalo.edu

^{*}To whom correspondence should be addressed

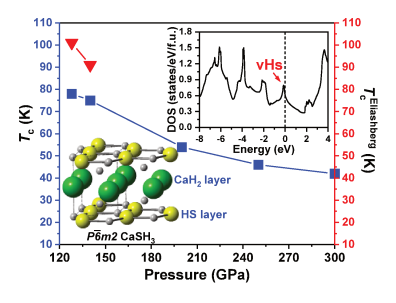
[†]Department of Chemistry, State University of New York at Buffalo, Buffalo, NY 14260-3000, USA

[‡]School of Sciences, Changchun University, Changchun, 130022, China

Abstract

Evolutionary searches predicted a number of ternary phases that could be synthesized at pressures of 100-300 GPa. $P6_3/mmc$ CaSH₂, Pnma CaSH₂, $Cmc2_1$ CaSH₆, and $I\bar{4}$ CaSH₂₀ were composed of a Ca-S lattice along with H₂ molecules coordinated in a "side-on" fashion to Ca. The H-H bond lengths in these semiconducting phases were elongated because of H₂ $\sigma \to$ Ca d donation, and Ca d \to H₂ σ^* back-donation, via a Kubas-like mechanism. $P\bar{6}m2$ CaSH₃, consisting of two-dimensional HS and CaH₂ sheets, was metastable and metallic above 128 GPa. The presence of van Hove singularities increased its density of states at the Fermi level, and concomitantly the superconducting critical temperature, which was estimated to be as high as \sim 100 K at 128 GPa. This work will inspire the search for superconductivity in materials based upon honeycomb HX (X=S, Se, Te), and MH₂ (M=Mg, Ca, Sr, Ba) layers under pressure.

TOC Graphic



The last years have witnessed tremendous advances in the search for conventional superconductivity in high pressure hydrides. ¹⁻⁹ First-principles based crystal structure prediction (CSP) techniques have pinpointed two classes of binary hydrides as being the most promising for high temperature superconductivity. ¹⁰ The first are composed of p-block elements in groups 13-16, such as the hydrides of phosphorus, ¹¹⁻¹⁴ and sulfur. ^{15,16} The second are alkaline or rare earth metal hydrides such as CaH₆, ¹⁷ which was predicted to have a superconducting critical temperature, T_c , of 220-235 K at 150 GPa. At the same time experiments have measured record breaking T_c values, first in $Im\bar{3}m$ H₃S (T_c of 203 K near 150 GPa) ¹⁸, and later in an $Fm\bar{3}m$ symmetry LaH₁₀ phase (T_c of 250-260 K near 200 GPa ^{19,20}) that was predicted prior to its synthesis. ^{21,22}

Ternary hydrides are the next frontier. Experimentally, only a few systems with low T_c s have been studied. ^{23,24} The theoretical prediction of ternaries poses considerable challenges because of the combinatorial complexity, wide stoichiometry range, and potentially large unit cell sizes. At the same time, the vast parameter space tantalizes at the prospect of discovering a stable or metastable species that has a high T_c at mild pressures. To date computations have predicted only a handful of ternaries with T_c s larger than 100 K, including LiPH₆ (167 K at 200 GPa), ²⁵ LiP₂H₁₄ (169 K at 230 GPa), ²⁶ Li₂MgH₁₆ (473 K at 250 GPa), ²⁷ CH₄-SH₃ (194 K at 150 GPa, ²⁸ or 181 K at 100 GPa²⁹), SH₃-SeH₃ (196 K at 200 GPa), ³⁰ MgCH₄ (121 K at 105 GPa), ³¹ H₃P_{0.15}S_{0.85} (197 K at 200 GPa), ³² and CaYH₁₂ (258 K at 200 GPa). ³³ However, with notable exceptions, ^{25–29} CSP searches were not carried out for a broad range of potential stoichiometries, and only a few compositions were considered.

Herein, CSP searches using the XTALOPT evolutionary algorithm (EA)^{34–36} coupled with Density Functional Theory (DFT) calculations were carried out to search for stable and intriguing metastable ternary hydrides (see the Supplementary Information, SI, for the computational details). Inspired by the high T_c values predicted for CaH₆,¹⁷ as well as those computed ¹⁵ and measured ¹⁸ in H₃S, we focused on the Ca-S-H system. EA runs were carried out on CaS and CaSH_n (n = 1-4, 6, 8, 9, 12, 18, 20) with 1-4 formula units comprising the unit cell at 100, 150, 200, 250 and 300 GPa. We found stable n = 2, 6, 20 phases composed of a Ca-S lattice wherein the

Ca ions were surrounded "side-on" by H_2 molecules that underwent $H_2 \sigma \to Ca d$ donation, and $Ca d \to H_2 \sigma^*$ back-donation. These phases were unlikely to be good superconductors. $P\bar{6}m2$ CaSH₃ contained CaH₂ layers, and two dimensional HS honeycomb sheets. Remarkably, just as in H_3S , the density of states at the Fermi level in $P\bar{6}m2$ CaSH₃ lies on a peak due to two van Hove singularities, thereby increasing its T_c , which was estimated to be as high as 94-101 K at 128 GPa.

CaS undergoes a $B1 \to B2$ phase transition near 40 GPa, ³⁷ and experiments have shown this structure is retained to 150 GPa. ³⁸ Accordingly, our EA searches at 100 and 150 GPa identified the B2 phase as being the most stable. Above 170 GPa $I4_1/amd$ CaS, see Fig. 1(a), emerged as the global minimum, and phonon calculations showed it was dynamically stable to at least 300 GPa (Figs. S5 and S7). $I4_1/amd$ CaS is composed of two interpenetrating Ca and S lattices that are both isotypic to a previously proposed phase of atomic metallic hydrogen. ³⁹ Analysis of the electronic structure showed that the bonding is fully ionic, and PBE calculations suggested this phase may be a weak metal at 170 GPa with pressure induced band broadening increasing the number of bands that cross the Fermi level, E_F (Fig. S6).

Since this study is concerned with compounds having the $CaSH_n$ stoichiometry, which could be synthesized from CaS and H_2 , we analyzed the 2D convex hulls that plot the enthalpy of formation, ΔH , from these two starting materials between 100-300 GPa (Fig. 2). The stoichiometries that lay on the 2D hull within the whole pressure range considered were $CaSH_2$, $CaSH_6$ and $CaSH_{20}$. Generally speaking the same species comprised the 3D hull (Fig. S2), the only exception being that the reaction $CaSH_{20} \rightarrow CaH_{12} + H_3S + 2.5H_2$ was favored by 7 meV/atom at 250 GPa, and $CaSH_{20} \rightarrow CaH_9 + H_3S + 4H_2$ was favored by 23 meV/atom at 300 GPa, within the static lattice approximation. When the zero-point-energy (ZPE) was taken into consideration (Fig. S3), $CaSH_{20}$ rose by no more than 4 meV/atom above the 2D hull at 100-250 GPa. By 128 GPa the $CaSH_3$ stoichiometry emerged as being metastable. When ZPE corrections were considered it lay 3-28 meV/atom above the 150-250 GPa 2D hulls, and it fell on the 300 GPa hull. Recent research on binary hydrides under pressure have shown that enthalpies calculated within the static-lattice approximation cannot be employed as the only predictors of synthesizability. Experimental pa-

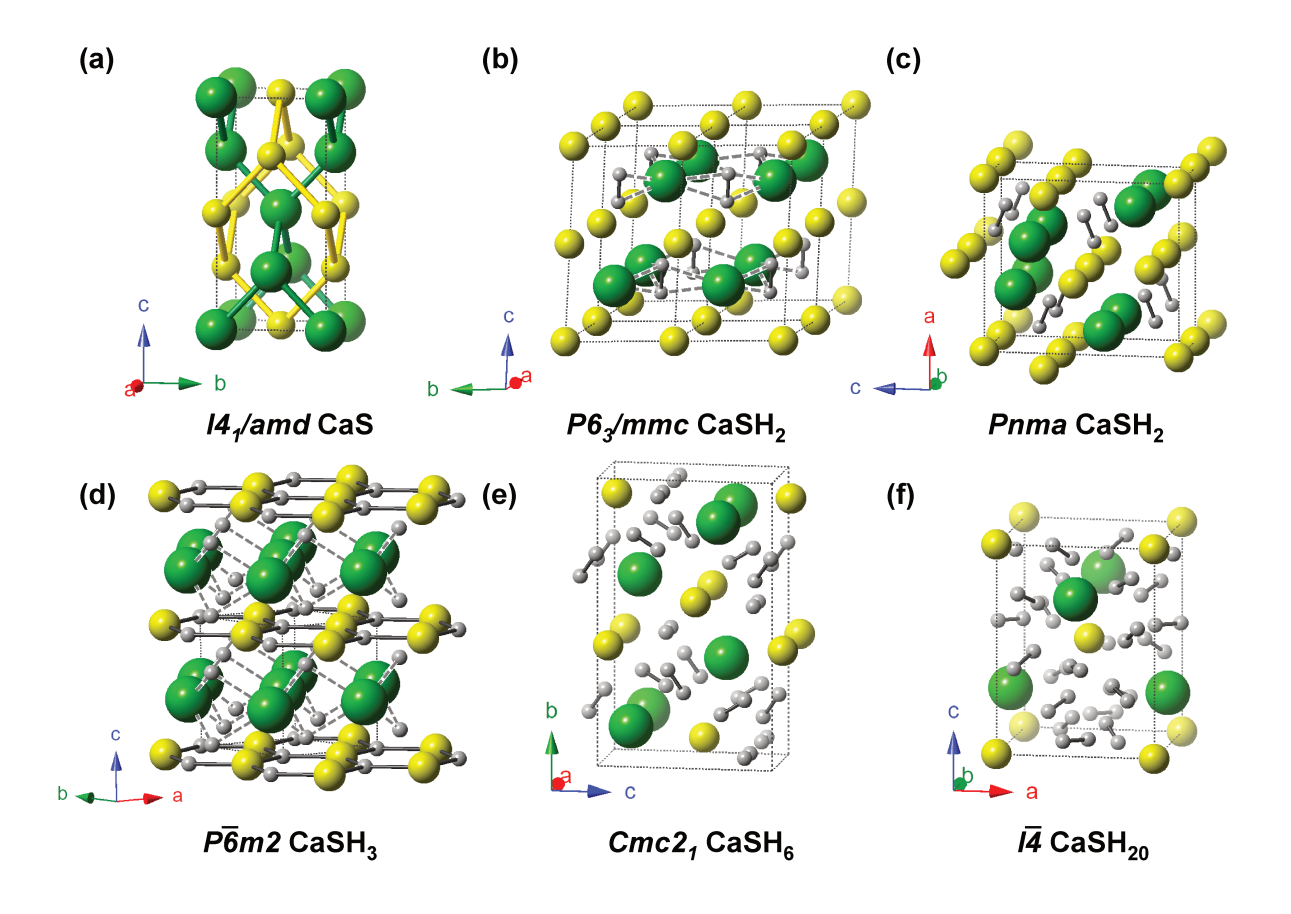


Figure 1: Crystal structures of predicted $CaSH_n$ phases under pressure: (a) tetragonal $I4_1/amd$ CaS, (b) hexagonal $P6_3/mmc$ $CaSH_2$, (c) orthorhombic Pnma $CaSH_2$, (d) hexagonal $P\bar{6}m2$ $CaSH_3$, (e) orthorhombic $Cmc2_1$ $CaSH_6$, and (f) tetragonal $I\bar{4}$ $CaSH_{20}$. Ca/S/H atoms are colored green/yellow/white. The solid lines connecting select hydrogen atoms indicate a bond, otherwise dashed lines are provided to guide the eye.

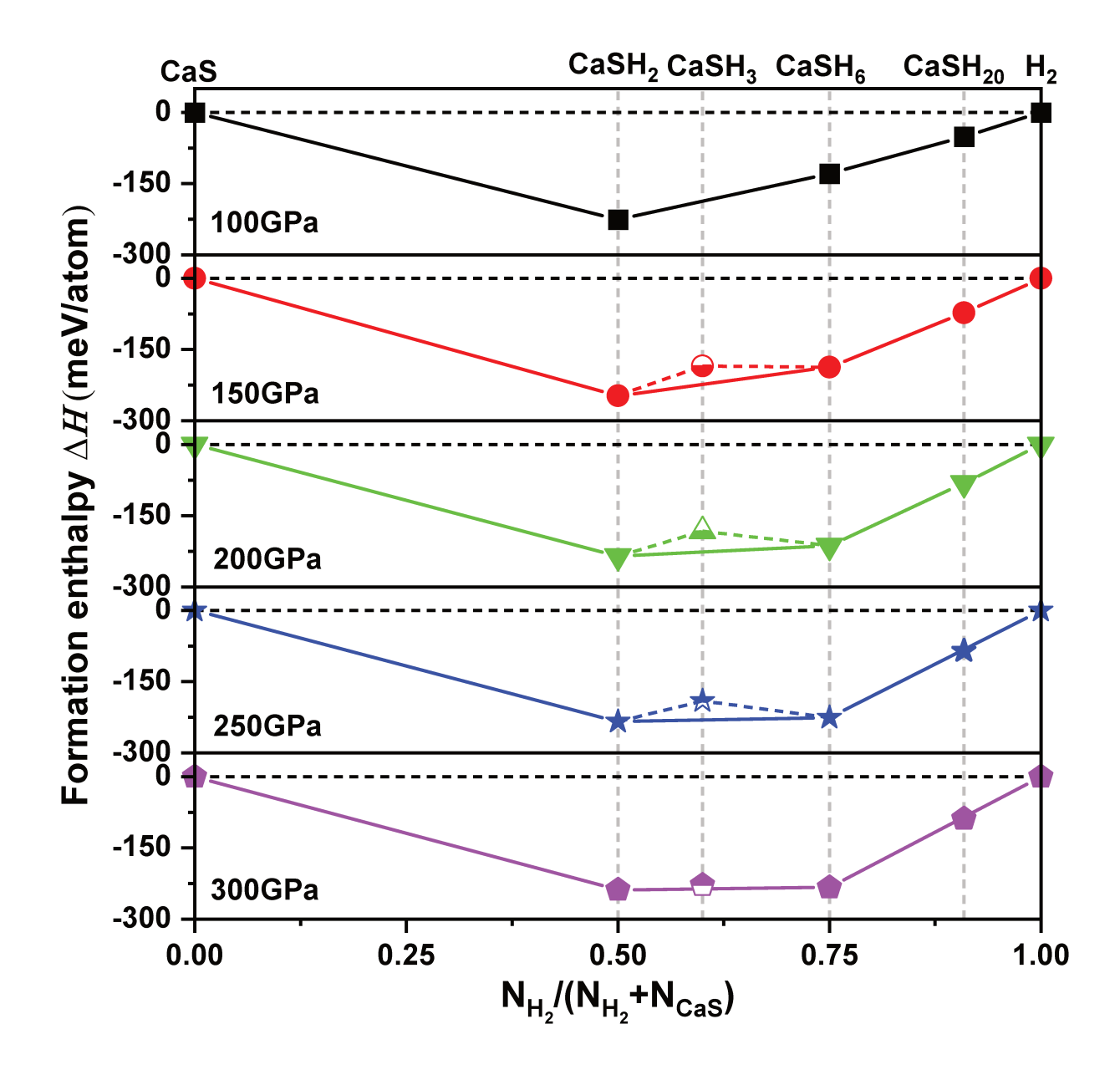


Figure 2: ΔH for the reaction $(\frac{1}{2}H_2)_n + \text{CaS} \to \text{CaSH}_n$ versus the mole fraction of H_2 in the ternary as a function of pressure. For H_2 we used the enthalpy of the C2/c (100-250 GPa) and Cmca-12 (300 GPa) phases, ⁴⁰ and for CaS the $Pm\bar{3}m$ (100-150 GPa), ³⁷ and $I4_1/amd$ (200-300 GPa) phases. Solid symbols lie on the convex hull (denoted by the solid lines), open symbols represent points above it. The ZPE-corrected convex hulls are given in Fig. S3.

rameters including the choice of the precursors and temperatures employed can be tuned to obtain various kinetically stable products. For example, the preparation temperature was the key variable controlling if the H₂S sample employed by Drozdov and co-workers persisted, or decomposed into H₃S. ¹⁸ Moreover, DFT calculations performed with classical nuclei have shown that the enthalpy

of the $Fm\bar{3}m$ LaH₁₀ phase is higher than that of other less symmetric structural alternatives, and it is dynamically unstable within the pressure range that superconductivity has been measured. ^{19,20} However, a recent theoretical study illustrated that anharmonic and quantum nuclear effects stabilize this phase, yielding computed T_c s consistent with experiment. ⁴² Therefore, both the stable and low-lying metastable Ca-S-H phases illustrated in Fig. 1 will be considered herein.

Between 100-160 GPa CaSH₂ adopts the $P6_3/mmc$ symmetry structure, composed of honeycomb layers wherein each Ca is coordinated to three H₂ molecules in a "side-on" fashion, and the S atoms are found in layers above and below the centers of the hexagons (Fig. 1(b)). Pnma CaSH₂, stable at higher pressures, can be derived via a distortion of the hexagonal phase that reduces its volume (19.68 Å³/f.u. vs. 20.42 Å³/f.u. at 300 GPa) (Fig. 1(c)). Throughout the whole pressure range studied $CaSH_6$ and $CaSH_{20}$ adopted the $Cmc2_1$ and $I\bar{4}$ spacegroups, respectively (Fig. 1(e) and (f)). Both were also characterized by Ca surrounded "side-on" by H_2 molecules. The "side-on" coordination of Ca by H₂ was first observed in an I4/mmm symmetry CaH₄ phase that was theoretically predicted ¹⁷ prior to its synthesis. ⁴³ This phase can be thought of as (CaH₂)(H₂)₂ whose H-H bond lengths were computed to be somewhat longer than those within solid H₂ at the same pressure. Detailed theoretical calculations showed that the increased bond length can be explained via a Kubas-like 44 mechanism wherein H_2 donates σ electrons to a vacant Ca d-orbital, and back-bonding from an occupied Ca d-orbital to the H_2 σ^* further weakens the H-H bond. ⁴³ Pressure is known to induce $s \to d$ transfer in Ca^{45} so, like in CaH_4 , the occupied Ca states in $CaSH_n$ are primarily d-like (Fig. S12). To further investigate if this mechanism occurs within the ternaries we calculated the negative of the crystal orbital Hamilton population integrated to the Fermi level (-ICOHP) for select atom pairs since it is a measure of their bond strength (Table 1).

Most of the H-H bond lengths in $P6_3/mmc$ and Pnma CaSH₂, $Cmc2_1$ CaSH₆ and $I\bar{4}$ CaSH₂₀ are longer than those computed for molecular H₂ at the same pressure. Table 1 shows that the H-H bond strength is smaller in these phases than in H₂ molecules that adopt the CaSH_n structure, but where the Ca and S atoms have been removed. The reason for this is that H₂ $\sigma \to$ Ca d donation, and Ca $d \to$ H₂ σ^* back-donation (Fig. S13) weakens the H-H bond in these ternaries, in-line with

the findings for CaH₄. ⁴³ The Bader charges illustrate that S becomes negatively charged because of electron transfer from Ca, and accordingly the interaction between these two atoms, as gauged by the -ICOHPs, is non-negligible, and even larger than in CaS at comparable pressures. The H-S bond strength is of a similar magnitude as the Ca-S interaction, and the markedly smaller H-Ca interaction is on par with results obtained previously for CaH₄. ⁴³

A number of hydrogenic motifs have been found in binary hydrides of the alkali, alkaline and rare earth metals under pressure. ¹⁰ The presence of $H_2^{\delta-}$ units, whose bonds were slightly elongated relative to the elemental phase, typically yielded good metals with moderate T_c s. ¹⁰ Phases where other species, such as H^- or H_3^- , were present along with H_2 , were usually insulators or weak metals. ^{2,3} Similar to the results obtained for $(CaH_2)(H_2)_2$, ⁴³ we speculated that the ternary hydrides, whose formulae can be written as $(Ca^{2+}S^{2-})(H_2)_n$ in the full ionic picture, were unlikely to have an electronic structure that was conducive towards superconductivity. Band structure calculations carried out with the PBE functional suggested that Pnma CaSH₂ at 300 GPa, and $I\bar{4}$ CaSH₂₀ at 200 GPa might be weak metals (Fig. S9). However, HSE06 screened hybrid functional calculations, which provide better estimates of the band gap, yielded gaps of \sim 0.4 eV (Fig. S10). This suggests that ternary hydrides containing an electropositive Group I, II or III element, combined with a p-block element are unlikely to be good superconductors if the only hydrogenic species found within them are H_2 units.

Three CaSH₃ lattices emerged as being the most stable in our EA searches at different pressures (Fig. S8). $P\bar{6}m2$ CaSH₃ (Fig. 1(d)) lay on the 300 GPa 2D hull including the ZPE (Fig. S3). At pressures smaller than ~240 GPa other phases had lower enthalpies, but $P\bar{6}m2$ CaSH₃ remained dynamically stable to 128 GPa. Molecular dynamics simulations (Section S18) at 240 and 140 GPa showed that this phase is thermally stable, as it did not undergo any structural reconstructions, thereby suggesting that it can be quenched to lower pressures. $P\bar{6}m2$ CaSH₃ did not contain any H₂ molecules, and it was composed of honeycomb SH layers wherein each S atom was bonded to three H atoms (and vice versa), and CaH₂ layers, so its formula can be written as (CaH₂)(SH). $Im\bar{3}m$ H₃S can be described as two interpenetrating SH₃ perovskite sublattices, wherein each S is

Table 1: Distances between select atom pairs in $Pm\bar{3}m$ and $I4_1/amd$ CaS, R3m and $Im\bar{3}m$ H₃S, I4/mmm CaH₄, $P6_3/mmc$ and Pnma CaSH₂, $Cmc2_1$ CaSH₆, $I\bar{4}$ CaSH₂₀ and their corresponding crystal orbital Hamilton populations integrated to the Fermi level (-ICOHPs) at various pressures. The -ICOHP for a hypothetical lattice of H₂ molecules where the Ca and S atoms are deleted are provided in parentheses. The H-H distance in solid molecular H₂ at 150, 200 and 300 GPa is 0.742, 0.745 and 0.756 Å, with corresponding -ICOHPs of 6.74, 6.62, and 6.21 eV/bond.

System	Space group	Pressure (GPa)	Atom Pairs	Distance (Å)	-ICOHP (eV/bond)
CaS	$Pm\bar{3}m$	150	Ca-S	2.419	0.40
	$I4_1/amd$	200	Ca-S	2.336	0.10
		250	Ca-S	2.295	0.13
		300	Ca-S	2.262	0.28
H_3S	R3m	150	H-S	1.458	4.16
	$Im\bar{3}m$	200	H-S	1.492	3.51
		300	H-S	1.433	3.73
CaH ₄	I4/mmm	120	Н-Н	0.811	4.15
			H _{atomic} -Ca	1.901	0.24
			H _{molecular} -Ca	2.048	0.11
			H _{molecular} -Ca	2.124	0.16
CaSH ₂	$P6_3/mmc$	150	Н-Н	0.811	3.92 (5.31)
			H-S	2.117	0.38
			Ca-S	2.340	0.65
			H-Ca	1.898	0.09
$CaSH_2$	Pnma	300	Н-Н	0.814	3.61 (5.51)
			H-S	1.745	0.84
			Ca-S	2.202	0.77
			H-Ca	1.766	0.09
$CaSH_3$	$P\bar{6}m2$	300	H-S	1.531	2.22
			H-S	1.704	1.01
			Ca-S	2.289	0.44
			H-Ca	1.803	0.18
$CaSH_6$	$Cmc2_1$	300	H-H	0.770	4.43 (5.41)
			H-H	0.776	4.25 (5.16)
			H-S	1.694	1.25
			Ca-S	2.276	0.72
			Ca-S	2.288	0.73
			H-Ca	1.743	0.12
$CaSH_{20}$	$I\bar{4}$	200	Н-Н	0.736	5.50 (6.29)
			H-H	0.750	5.26 (6.01)
			Н-Н	0.760	4.89 (6.02)
			H-S	1.744	1.33
			Ca-S	2.592	0.50
			H-Ca	1.863	0.15

octahedrally coordinated by H, and each H is coordinated to two S atoms. ¹⁵ The nearest neighbor H-S bond lengths in $P\bar{6}m2$ CaSH₃, 1.531 Å at 300 GPa, are somewhat longer and weaker than those in SH₃ at the same pressure, 1.433 Å (-ICOHPs of 2.22 vs. 3.73 eV/bond). Below we investigate if other characteristics of $P\bar{6}m2$ CaSH₃ bear a resemblance to those computed for superconducting H₃S.

The projected density of states (DOS) at 250 GPa, and the corresponding band structure projected onto atomic orbitals (fat bands) of $P\bar{6}m2$ CaSH₃ are plotted in Fig. 3. They show that Ca d, S p and H s states are found to give the largest contributions to the DOS at $E_{\rm F}$. There are twice as many hydrogen atoms in the CaH₂ layers as compared with the SH layers, so it is no surprise that the DOS is larger for the former than the latter. However, along the high symmetry lines crossing $E_{\rm F}$ the character is primarily due to the CaH₂ hydrogens, and the band just below $E_{\rm F}$ at the A-point contains character from both (Fig. S11). Remarkably, the DOS at $E_{\rm F}$ lies close to the top of a particularly sharp peak that is due to two van Hove singularities (vHs) separated by \sim 64 meV (Fig. S24). Because vHs increase the number of states at $E_{\rm F}$ that can participate in the electronphonon-coupling (EPC) mechanism, they are known to enhance the total coupling strength, λ , and in turn the T_c in conventional superconductors. It is therefore not surprising that DFT calculations showed that $Im\bar{3}m$ H₃S and $Fm\bar{3}m$ LaH₁₀ exhibit such double-shaped vHs at $E_{\rm F}$ separated by \sim 300 meV 46 and \sim 90 meV, 47 respectively. The role that vHs play in increasing the T_c in H₃S has been studied in great detail. $^{46,48-50}$ Between 128-300 GPa the vHs in CaSH $_3$ are pinned near $E_{\rm F}$ (Fig. S14), and the Fermi surface remains nearly invariant (Figs. S20-S23). By 140 GPa, however, a band that displays H s character rises above $E_{\rm F}$ at the A-point, resulting in a Lifshitz transition. As shown in Table 2, the Lifshitz transition is associated with a pronounced increase of the DOS at $E_{\rm F}$, suggesting that T_c may be largest near the onset of dynamic instability, which occurs near 128 GPa (Fig. S25).

Subsequently, we calculated the phonon band structures, projected phonon DOS, Eliashberg spectral function, $\alpha^2 F(\omega)$, and the EPC integral, $\lambda(\omega)$, for $P\bar{6}m2$ CaSH₃ within the range of its dynamic stability (Figs. 4, S25 and S26). At 250 GPa two gaps separate the phonon spectrum into

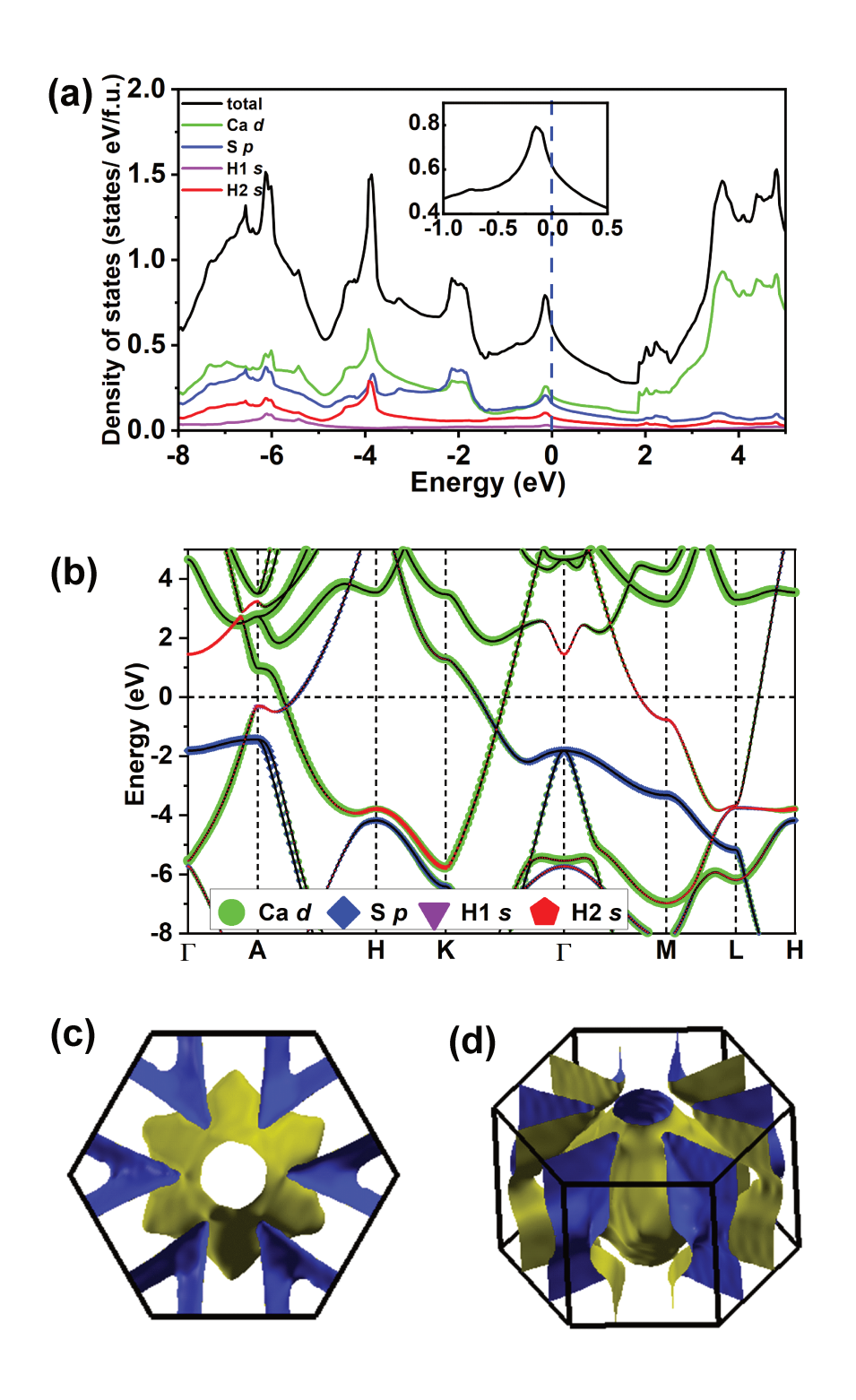


Figure 3: The electronic structure of $P\bar{6}m2$ CaSH₃ at 250 GPa: (a) projected density of states (DOS), with the inset showing a blow up around the Fermi level, (b) fat bands illustrating the character arising from the H1/H2 s states (also see Fig. S11), S p states, and Ca d states, and (c,d) Fermi surface – top and side view. H1 atoms are in the "SH" layers, and H2 atoms are in the "CaH₂" layers (see Fig. 1(d)).

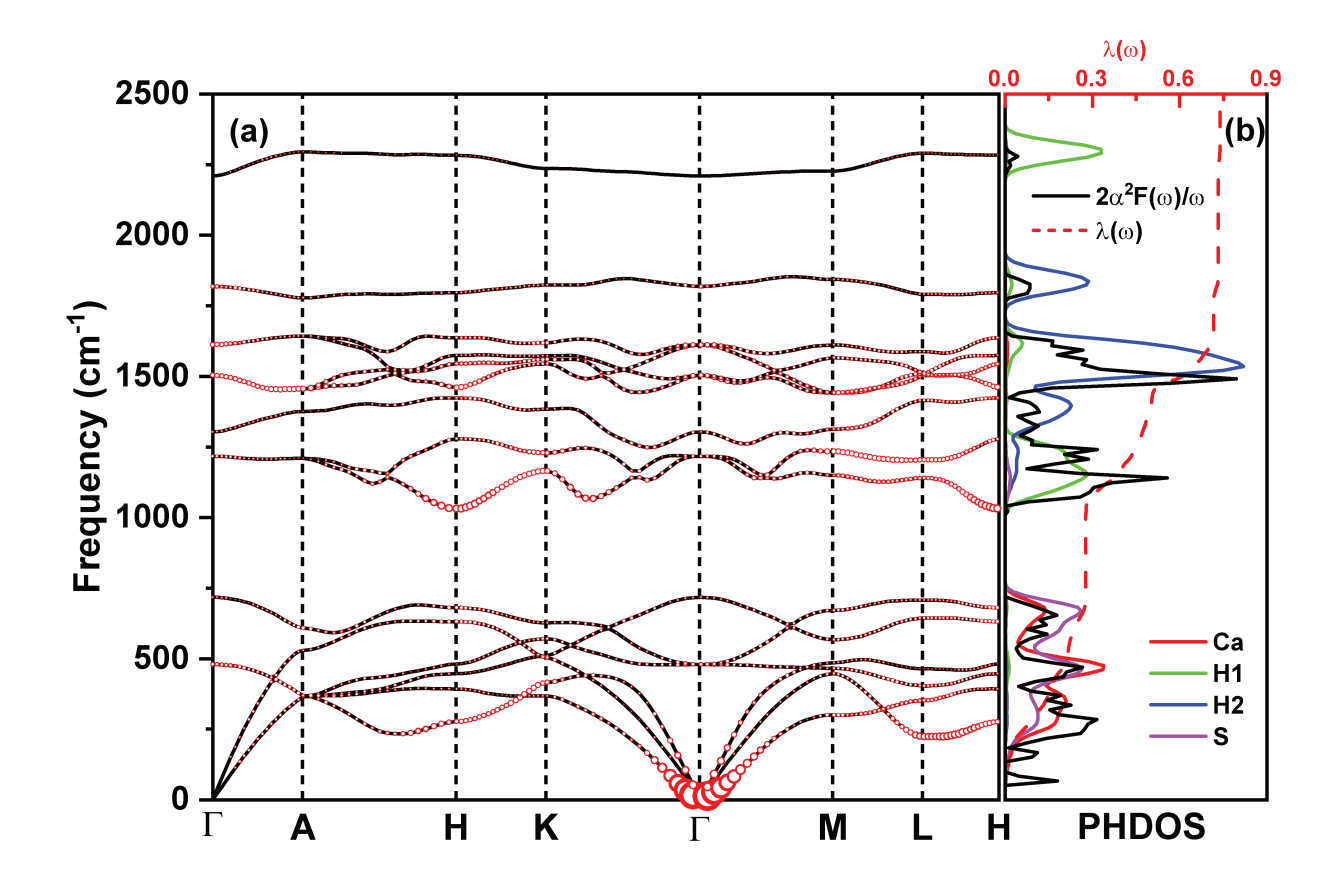


Figure 4: Superconducting properties of $P\bar{6}m2$ CaSH₃ at 250 GPa: (a) phonon band structure where the radius of the circles is proportional to the electron-phonon coupling constant, $\lambda_{\mathbf{q}\nu}$, for mode ν at wavevector \mathbf{q} (phonon linewidth), and (b) the Eliashberg spectral function (black line), electron phonon integral, $\lambda(\omega)$ (red dashed line), and projected phonon densities of states (PHDOS). H1 atoms are in the "SH" layers, and H2 atoms are in the "CaH₂" layers (see Fig. 1(d)).

three regions: the lower frequency modes are mainly associated with the motions of the heavier calcium and sulfur atoms, while the hydrogens in the SH layers (H1) and those in the CaH₂ layers (H2) contribute to the intermediate region, and the higher frequency modes are associated with the H1 atoms, with these regions contributing 37.6, 59.4, and 3% to the total λ , respectively. Most of the phonon modes harden up to 300 GPa resulting in an increased logarithmic average of phonon frequencies, ω_{log} . On the other hand, the EPC increases with decreasing pressure, attaining a maximum value of $\lambda = 1.64$ at 128 GPa. T_c was estimated using the Allen-Dynes modified McMillan equation, ⁵¹ along with typical values of the renormalized Coulomb repulsion, $\mu^* = 0.1 - 0.13$, and it was found to fall in the range of 36-46 K at 250 GPa, increasing to 66-75 K by 140 GPa (Table 2). It is well-known that for strongly coupled systems, $\lambda \gtrsim 1.5$, this method underestimates T_c . Numerically solving the Eliashberg equations provides a more accurate estimate, resulting in values as high as 94-101 K at 128 GPa.

The phonon linewidths illustrate that many modes in the low and intermediate frequency regions contribute towards λ . A set of modes around, but not at, Γ along the $K-\Gamma-M$ path stand out as having particularly large linewidths. Their frequencies are degenerate with one of the translational modes that corresponds to displacement of the 2D layers in the xy plane. Visualization of two arbitrarily chosen modes on the $K-\Gamma$ and $\Gamma-M$ paths with large linewidths show that all of the atoms move in the xy plane. Both modes are reminiscent of planewaves, but locally the motion along $K-\Gamma$ resembles rocking, and the one along $\Gamma-M$ scissoring. The phonon band structure at 128 GPa is not too different from the one at 250 GPa, except that the division into three separate regions is not so obvious because of the softening of the modes in the intermediate regime (Figs. S25 and S26). In addition to the modes along the $K-\Gamma-M$ high symmetry lines softened modes along the A-H and A-H paths also possess a large linewidth. At lower pressures the latter become imaginary, and the phase becomes dynamically unstable.

Since $P\bar{6}m2$ CaSH₃ can be thought of as 2D SH layers sandwiched between CaH₂ sheets, it is instructive to compare its predicted superconducting properties with similar systems. The maximum EPC parameter calculated for CaSH₃, $\lambda = 1.64$, is lower than that of the strongly coupled

 H_3S phases, 15 as is ω_{log} resulting in a T_c that is about a factor of two smaller. The EPC in a family of superconducting ternary hydrides based on an H_3S lattice intercalated by CH_4 ranged from $\lambda=1.06-3.64$, and T_c , as calculated using the Allen-Dynes modified McMillan equation with $\mu^*=0.1$, fell between 98-156 K. 28,29 Whereas the DOS at E_F in CH_4 - SH_3 only contained contributions from the H_3S framework, in $CaSH_3$ substantial Ca d-character was also present. Therefore, despite the presence of vHs near E_F in both $CaSH_3$ and H_3S , the microscopic mechanism of superconductivity in these two phases is subtly different, whereas only the H_3S lattice contributes to the superconductivity in CH_4 - SH_3 .

Table 2: Superconducting parameters for $P\bar{6}m2$ CaSH $_3$ at various pressures: electron-phonon coupling parameter (λ), logarithmic average of phonon frequencies (ω_{\log}) and estimated superconducting critical temperature (T_c) for values of the Coulomb pseudopotential, μ^* , of 0.1 and 0.13 using the Allen-Dynes modified McMillan equation ⁵¹ (and numerically solving the Eliashberg equations ⁵²). The density of states at the Fermi level, $N(E_{\rm F})$, is also provided in units of states/eV/f.u.

Pressure (GPa)	λ	$\omega_{\log}(\mathbf{K})$	$T_c^{\mu^* = 0.1} (K)$	$T_c^{\mu^* = 0.13}$ (K)	$N(E_f)$
128	1.64	629.6	78 (101)	71 (94)	0.74
140	1.18	861.2	75 (91)	66 (82)	0.72
200	0.82	1102.1	54	44	0.64
250	0.74	1170.5	46	36	0.61
300	0.70	1211.0	42	32	0.59

In conclusion, evolutionary searches have identified five hitherto unknown phases with unique stoichiometries in the ternary Ca-S-H system that may be synthesizable at pressures of 100-300 GPa. $P6_3/mmc$ CaSH₂, Pnma CaSH₂, $Cmc2_1$ CaSH₆, and $I\bar{4}$ CaSH₂₀, which comprise the 2D convex hull, contain Ca, S and H₂ molecules. The H-H distances in these semiconductors are elongated as compared to molecular H₂ because of H₂ $\sigma \rightarrow$ Ca d donation, and Ca $d \rightarrow$ H₂ σ^* back-donation via a Kubas-like mechanism. Moreover, we also predict a metallic $P\bar{6}m2$ CaSH₃ phase composed of 2D honeycomb HS layers separated by layers of CaH₂ that is metastable between 128-300 GPa. The DOS at E_F , which exhibits Ca d, S p and H s character, lies near a peak that is due to two van Hove singularities (vHs). Remarkably, E_F remains pinned at the vHs, and the Fermi surface is nearly invariant within the range of dynamic stability. By 140 GPa a new band

rises above $E_{\rm F}$ resulting in a Lifshitz transition that markedly increases the DOS at $E_{\rm F}$, and concomitantly the EPC. Estimates of the T_c via the Allen-Dynes modified McMillan equation range from 32-42 K at 300 GPa, whereas numerically solving the Eliashberg equations suggests T_c may be as high as 94-101 K at 128 GPa. Our findings provide a microscopic understanding of the superconducting mechanism in $P\bar{6}m2$ CaSH₃, and inspire the search for superconductivity in phases composed of honeycomb HX (X=S, Se, Te), and MH₂ (M=Mg, Ca, Sr, Ba) layers. For example, exploratory calculations (Section S19) shown that an isotypic CaSeH₃ phase is dynamically stable at pressures as low as 110 GPa. Its band structure resembles that of $P\bar{6}m2$ CaSH₃, except bands that are unoccupied in CaSH₃ cross E_F along the $\Gamma-A$ and $K-\Gamma-M$ high symmetry lines. We are looking forward to future work studying the effect of the chemical substitution on the stability and superconducting properties of phases isotypic with $P\bar{6}m2$ CaSH₃ under pressure.

Acknowledgements: This material is based upon work supported by the U.S. Department of Energy, Office of Science, Fusion Energy Sciences under Award No. DE-SC0020340 (Y.Y.). T.B., N.G., and X.W. acknowledge the U.S. National Science Foundation (DMR-1827815) for financial support. Calculations were performed at the Center for Computational Research at SUNY Buffalo. ⁵³ We thank Russell Hemley for helpful discussions.

Supporting Information: The Supporting Information is available free of charge on the ACS Publication website. It includes the computational details, illustrations of the 3D and 2D convex hulls, structural parameters, relative enthalpies, electronic band structures and densities of states, phonon band structures, electron localization functions, and Bader charges of select CaS and CaSH_n (n = 2, 3, 6, 20) phases, as well as the Fermi surface, isoenergy contours, snapshots of MD simulations, and Eliashberg spectral function of $P\bar{6}m2$ CaSH₃ at different pressures.

References

- (1) Struzhkin, V. V. Superconductivity in Compressed Hydrogen-Rich Materials: Pressing on Hydrogen. *Physica C* **2015**, *514*, 77–85.
- (2) Zurek, E. Hydrides of the Alkali Metals and Alkaline Earth Metals Under Pressure. *Comments Inorg. Chem.* **2017**, *37*, 78–98.
- (3) Shamp, A.; Zurek, E. Superconductivity in Hydrides Doped with Main Group Elements Under Pressure. *Nov. Supercond. Mater.* **2017**, *3*, 14–22.
- (4) Duan, D.; Liu, Y.; Ma, Y.; Shao, Z.; Liu, B.; Cui, T. Structure and Superconductivity of Hydrides at High Pressures. *Natl. Sci. Rev.* **2016**, *4*, 121–135.
- (5) Wang, H.; Li, X.; Gao, G.; Li, Y.; Ma, Y. Hydrogen–Rich Superconductors at High Pressures. Wiley Interdiscip. Rev. Comput. Mol. Sci. 2017, 8, 1–13.
- (6) Pickard, C. J.; Errea, I.; Eremets, M. I. Superconducting Hydrides Under Pressure. *Annu. Rev. Condens. Matter Phys.* **2019**, *11*, 57–76.
- (7) Flores-Livas, J. A.; Boeri, L.; Sanna, A.; Profeta, G.; Arita, R.; Eremets, M. A Perspective on Conventional High-Temperature Superconductors at High Pressure: Methods and Materials. *Phys. Rep.* 2020, 856, 1–78.
- (8) Bi, T.; Zarifi, N.; Terpstra, T.; Zurek, E. In *Elsevier Reference Module in Chemistry, Molecular Sciences and Chemical Engineering*; Reedijk, J., Ed.; Elsevier: Waltham, MA, 2019; pp 1–36.
- (9) Semenok, D. V.; Kruglov, I. A.; Savkin, I. A.; Kvashnin, A. G.; Oganov, A. R. On Distribution of Superconductivity in Metal Hydrides. *Curr. Opin. Solid State Mater. Sci.* **2020**, *24*, 100808.
- (10) Zurek, E.; Bi, T. High-Temperature Superconductivity in Alkaline and Rare Earth Polyhydrides at High Pressure: A Theoretical Perspective. *J. Chem. Phys.* **2019**, *150*, 050901.

- (11) Shamp, A.; Terpstra, T.; Bi, T.; Falls, Z.; Avery, P.; Zurek, E. Decomposition Products of Phosphine Under Pressure: PH₂ Stable and Superconducting? *J. Am. Chem. Soc.* **2016**, *138*, 1884–1892.
- (12) Bi, T.; Miller, D. P.; Shamp, A.; Zurek, E. Superconducting Phases of Phosphorus Hydride Under Pressure: Stabilization via Mobile Molecular Hydrogen. *Angew. Chem. Int. Ed.* 2017, 56, 10192–10195.
- (13) Liu, H.; Li, Y.; Gao, G.; Tse, J. S.; Naumov, I. I. Crystal Structure and Superconductivity of PH₃ at High Pressures. *J. Phys. Chem. C* **2016**, *120*, 3458–3461.
- (14) Flores-Livas, J. A.; Amsler, M.; Heil, C.; Sanna, A.; Boeri, L.; Profeta, G.; Wolverton, C.; Goedecker, S.; Gross, E. K. U. Superconductivity in Metastable Phases of Phosphorus–Hydride Compounds Under High Pressure. *Phys. Rev. B* 2016, 93, 020508(R).
- (15) Duan, D.; Liu, Y.; Tian, F.; Li, D.; Huang, X.; Zhao, Z.; Yu, H.; Liu, B.; Tian, W.; Cui, T. Pressure-induced Metallization of Dense (H₂S)₂H₂ with High-T_c Superconductivity. Sci. Rep. 2014, 4, 6968.
- (16) Yao, Y.; Tse, J. S. Superconducting Hydrogen Sulfide. *Chem. Eur. J* **2018**, 24, 1769–1778.
- (17) Wang, H.; John, S. T.; Tanaka, K.; Iitaka, T.; Ma, Y. M. Superconductive sodalite-like clathrate calcium hydride at high pressures. *Proc. Natl. Acad. Sci. USA* **2012**, *109*, 6463–6466.
- (18) Drozdov, A. P.; Eremets, M. I.; Troyan, I. A.; Ksenofontov, V.; Shylin, S. I. Conventional Superconductivity at 203 Kelvin at High Pressures in the Sulfur Hydride System. *Nature* **2015**, *525*, 73–76.
- (19) Somayazulu, M.; Ahart, M.; Mishra, A. K.; Geballe, Z. M.; Baldini, M.; Meng, Y.; Struzhkin, V. V.; Hemley, R. J. Evidence for Superconductivity above 260 K in Lanthanum Superhydride at Megabar Pressures. *Phys. Rev. Lett.* **2019**, *122*, 027001.

- (20) Drozdov, A. P.; Kong, P. P.; Minkov, V. S.; Besedin, S. P.; Kuzovnikov, M. A.; Mozaffari, S.; Balicas, L.; Balakirev, F. F.; Graf, D. E.; Prakapenka, V. B. Superconductivity at 250 K in Lanthanum Hydride Under High Pressures. *Nature* **2019**, *569*, 528–531.
- (21) Liu, H. Y.; Naumov, I. I.; Hoffmann, R.; Ashcroft, N. W.; Hemley, R. J. Potential High-T_c Superconducting Lanthanum and Yttrium Hydrides at High Pressure. *Proc. Natl. Acad. Sci. U.S.A.* 2017, 114, 6990–6995.
- (22) Peng, F.; Sun, Y.; Pickard, C. J.; Needs, R. J.; Wu, Q.; Ma, Y. Hydrogen Clathrate Structures in Rare Earth Hydrides at High Pressures: Possible Route to Room-Temperature Superconductivity. *Phys. Rev. Lett.* **2017**, *119*, 107001.
- (23) Muramatsu, T.; Wanene, W. K.; Somayazulu, M.; Vinitsky, E.; Chandra, D.; Strobel, T. A.; Struzhkin, V. V.; Hemley, R. J. Metallization and Superconductivity in the Hydrogen-Rich Ionic Salt BaReH₉. J. Phys. Chem. C 2015, 119, 18007–18013.
- (24) Meng, D.; Sakata, M.; Shimizu, K.; Iijima, Y.; Saitoh, H.; Sato, T.; Takagi, S.; Orimo, S.i. Superconductivity of the Hydrogen-Rich Metal Hydride Li₅MoH₁₁ Under High Pressure. *Phys. Rev. B* 2019, 99, 024508.
- (25) Shao, Z.; Duan, D.; Ma, Y.; Yu, H.; Song, H.; Xie, H.; Li, D.; Tian, F.; Liu, B.; Cui, T. Ternary Superconducting Cophosphorus Hydrides Stabilized via Lithium. *NPJ Comput. Mater.* **2019**, *5*, 104.
- (26) Li, X.; Xie, Y.; Sun, Y.; Huang, P.; Liu, H.; Chen, C.; Ma, Y. Chemically Tuning Stability and Superconductivity of PH Compounds. *J. Phys. Chem. Lett.* **2020**, *11*, 935–939.
- (27) Sun, Y.; Lv, J.; Xie, Y.; Liu, H.; Ma, Y. Route to a Superconducting Phase above Room Temperature in Electron-Doped Hydride Compounds Under High Pressure. *Phys. Rev. Lett.* **2019**, *123*, 097001.

- (28) Cui, W.; Bi, T.; Shi, J.; Li, Y.; Liu, H.; Zurek, E.; Hemley, R. J. Route to High- T_c Superconductivity via CH₄ Intercalated H₃S Hydride Perovskites. *Phys. Rev. B* **2020**, *101*, 134504.
- (29) Sun, Y.; Tian, Y.; Jiang, B.; Li, X.; Li, H.; Iitaka, T.; Zhong, X.; Xie, Y. Computational Discovery of a Dynamically Stable Cubic SH₃-Like High-Temperature Superconductor at 100 GPa via CH₄ Intercalation. *Phys. Rev. B* **2020**, *101*, 174102.
- (30) Liu, B.; Cui, W.; Shi, J.; Zhu, L.; Chen, J.; Lin, S.; Su, R.; Ma, J.; Yang, K.; Xu, M. et al. Effect of Covalent Bonding on the Superconducting Critical Temperature of the HS-Se System. *Phys. Rev. B* **2018**, *98*, 174101.
- (31) Tian, F.; Li, D.; Duan, D.; Sha, X.; Liu, Y.; Yang, T.; Liu, B.; Cui, T. Predicted Structures and Superconductivity of Hypothetical Mg-CH₄ Compounds Under High Pressures. *Mater. Res. Express* **2015**, *2*, 046001.
- (32) Fan, F.; Papaconstantopoulos, D. A.; Mehl, M. J.; Klein, B. M. High-Temperature Superconductivity at High Pressures for $H_3Si_xP_{1-x}$, $H_3P_xS_{1-x}$, and $H_3Cl_xS_{1-x}$. *J. Phys. Chem. Solids* **2016**, *99*, 105–110.
- (33) Liang, X.; Bergara, A.; Wang, L.; Wen, B.; Zhao, Z.; Zhou, X.-F.; He, J.; Gao, G.; Tian, Y. Potential High- T_c Superconductivity in CaYH₁₂ Under Pressure. *Phys. Rev. B* **2019**, *99*, 100505.
- (34) Lonie, D. C.; Zurek, E. XtalOpt: An open-source evolutionary algorithm for crystal structure prediction. *Comput. Phys. Commun.* **2011**, *182*, 372–387.
- (35) Avery, P.; Falls, Z.; Zurek, E. XTALOPT Version r10: An Open–Source Evolutionary Algorithm for Crystal Structure Prediction. *Comput. Phys. Commun.* **2017**, 217, 210–211.
- (36) Avery, P.; Falls, Z.; Zurek, E. XTALOPT Version r11: An Open–Source Evolutionary Algorithm for Crystal Structure Prediction. *Comput. Phys. Commun.* **2018**, 222, 418–419.
- (37) Luo, H.; Greene, R. G.; Ghandehari, K.; Li, T.; Ruoff, A. L. Structural Phase Transformations

- and the Equations of State of Calcium Chalcogenides at High Pressure. *Phys. Rev. B* **1994**, 50, 16232.
- (38) Ghandehari, K.; Akella, J.; Weir, S. T.; Ruddle, C. A. Ultrahigh Pressure Equation of State of CaS to 1.5 Mbar. *High Pressure Res.* **2001**, *21*, 31–40.
- (39) McMahon, J. M.; Ceperley, D. M. High-Temperature Superconductivity in Atomic Metallic Hydrogen. *Phys. Rev. B* **2011**, *84*, 144515.
- (40) Pickard, C. J.; Needs, R. J. Structure of phase III of solid hydrogen. *Nat. Phys.* **2007**, *3*, 473–476.
- (41) Liu, H.; Naumov, I. I.; Geballe, Z. M.; Somayazulu, M.; Tse, J. S.; Hemley, R. J. Dynamics and Superconductivity in Compressed Lanthanum Superhydride. *Phys. Rev. B* **2018**, *98*, 100102(R).
- (42) Errea, I.; Belli, F.; Monacelli, L.; Sanna, A.; Koretsune, T.; Tadano, T.; Bianco, R.; Calandra, M.; Arita, R.; Mauri, F. et al. Quantum Crystal Structure in the 250 Kelvin Superconducting Lanthanum Hydride. *Nature* **2020**, *578*, 66–69.
- (43) Mishra, A. K.; Muramatsu, T.; Liu, H.; Geballe, Z. M.; Somayazulu, M.; Ahart, M.; Baldini, M.; Meng, Y.; Zurek, E.; Hemley, R. J. New Calcium Hydrides with Mixed Atomic and Molecular Hydrogen. *J. Phys. Chem. C* **2018**, *122*, 19370–19378.
- (44) Kubas, G. J.; Ryan, R. R.; Swanson, B. I.; Vergamini, P. J.; Wasserman, H. J. Characterization of the First Examples of Isolable Molecular Hydrogen Complexes, M(CO)₃(PR₃)₂(H₂)(M= Molybdenum or Tungsten; R= Cy or Isopropyl). Evidence for a Side-On Bonded Dihydrogen Ligand. *J. Am. Chem. Soc.* **1984**, *106*, 451–452.
- (45) Maksimov, E. G.; Magnitskaya, M. V.; Fortov, V. E. Non-simple Behavior of Simple Metals at High Pressure. *Phys.-Usp.* **2005**, *48*, 761–780.

- (46) Quan, Y.; Pickett, W. E. Van Hove Singularities and Spectral Smearing in High-Temperature Superconducting H₃S. *Phys. Rev. B* **2016**, *93*, 104526.
- (47) Liu, L.; Wang, C.; Yi, S.; Kim, K. W.; Kim, J.; Cho, J. Microscopic Mechanism of Room-Temperature Superconductivity in Compressed LaH₁₀. *Phys. Rev. B* **2019**, *99*, 140501.
- (48) Sano, W.; Koretsune, T.; Tadano, T.; Akashi, R.; Arita, R. Effect of van Hove Singularities on High- T_c Superconductivity in H₃S. *Phys. Rev. B* **2016**, *93*, 094525.
- (49) Ortenzi, L.; Cappelluti, E.; Pietronero, L. Band Structure and Electron-Phonon Coupling in H₃S: A Tight-Binding Model. *Phys. Rev. B* **2016**, *94*, 064507.
- (50) Akashi, R. Archetypical "Push the Band Critical Point" Mechanism for Peaking of the Density of States in Three Dimensional Crystals: Theory and Case Study of Cubic H₃S. *Phys. Rev. B* **2020**, *101*, 075126.
- (51) Allen, P. B.; Dynes, R. C. Transition Temperature of Strong-Coupled Superconductors Reanalyzed. *Phys. Rev. B* **1975**, *12*, 905.
- (52) Eliashberg, G. M. Interactions Between Electrons and Lattice Vibrations in a Superconductor. *Sov. Phys. JETP* **1960**, *11*, 696–702.
- (53) http://hdl.handle.net/10477/79221, accessed July 05, 2020.